

Several Types of Antennas Composed of Microwave Metamaterials

Tie Jun CUI^{†a)}, Xiao-Yang ZHOU[†], Xin Mi YANG^{††}, Wei Xiang JIANG[†], Qiang CHENG[†],
and Hui Feng MA[†], *Nonmembers*

SUMMARY We present a review of several types of microwave antennas made of metamaterials, including the resonant electrically small antennas, metamaterial-substrate patch antennas, metamaterial flat-lens antennas, and Luneburg lens antennas. In particular, we propose a new type of conformal antennas using anisotropic zero-index metamaterials, which have high gains and low sidelobes. Numerical simulations and experimental results show that metamaterials have unique properties to design new antennas with high performance.

key words: metamaterials, resonant antennas, metamaterial substrate, gradient index, anisotropic zero index, flat lens, Luneburg lens, high performance

1. Introduction

Due to the unique and unusual properties which cannot be achieved by natural materials, metamaterials have attracted much attention in the scientific and engineering communities. Firstly known as the left-handed material (LHM) [1] which possess negative permittivity and negative permeability simultaneously, metamaterial has now become a much broader concept [2], including LHM, electric plasma, magnetic plasma, gradient-index (GRIN) material, and zero-index material, etc. Because of the outstanding performance of metamaterials, they have been used to design some exciting devices such as invisibility cloaks [3]–[8], ground-plane cloaks [9]–[13], electromagnetic concentrators [14], [15], rotators [16], polarizers [17]–[19], novel antennas [20]–[26], and optical-illusion devices [27]–[30].

Among the above-mentioned exciting devices, the novel antennas are of great importance due to their practical applications in microwave engineering. In the first part of the paper, we present a review of several types of antennas which are realized using the microwave metamaterials: the electrically small antennas made of metamaterial resonant structures, the patch antennas with the waveguided metamaterial substrates, the flat-lens antennas made of GRIN metamaterials, and the Luneburg lens antennas made of GRIN metamaterials. In the second part of the paper, we propose a

new type of conformal antennas using the anisotropic zero-index metamaterials, which have high gains and low sidelobes. Both numerical simulations and experimental results show that metamaterials have unique properties to design novel antennas with high performance.

2. Electrically-Small Antennas Composed of Metamaterial Unit Cells [31]

Resonant metamaterial unit cells can be used to reduce the antenna size while maintaining the satisfactory antenna performance. Mosallaei and Sarabandi introduced the concept of magneto-dielectrics design in 2004, which was proved to be effective in the patch antenna miniaturization [32]. Later, a metamaterial ring antenna was firstly proposed by Qureshi et al. with the efficiency of 54% [33]. The design of miniaturized metamaterial patch antenna was further proposed by Bilotti using the negative-permeability loading [34]. Recently, Ziolkowski and Erentok proposed an efficient approach to reduce the antenna size by matching the antenna with a metamaterial-inspired element [35], [36]. Here, we emphasize an electrically-small metamaterial antenna made on a printed planar structure.

Figure 1 shows a novel electrically small antenna based on the split-ring resonator (SRR) geometry [31]. It is a compact printed planar structure, including three parts: 1) the two radiation patches on the top of substrate [Fig. 1(a)]; 2) the metal vias integrated in the midlayer of the substrate as the metal walls [37] [Fig. 1(b)]; and 3) the CPW feed line in the ground plane [Fig. 1(c)] [31]. This antenna configuration is actually the extrusion of the conventional SRR structure [38], which is excited by a coplanar waveguide (CPW) line. The metal vias arranged along the edges of the radiation patch connect the top layer with the ground plane to form a series resonant circuit, enabling the antenna to operate at the wavelength much larger than its size. Meanwhile, the metal vias arranged along the gap between the two radiation patches act as perfectly electric conductor (PEC) wall in the substrate, which greatly increases the effective capacitance of the resonant circuit. Note that the areas, where the metal vias along the gap are connected to, are separated from the CPW ground plane to prevent short-circuiting of the resonant circuit. The extending of the top radiation patches efficiently capture the magnetic flux generated by the feed line and the antenna can be regarded as a magnetic dipole at resonance. The main radiation direction is normal to the radi-

Manuscript received October 4, 2010.

Manuscript revised November 18, 2010.

[†]The authors are with the State Key Laboratory of Millimeter Waves and the Institute of Target Characteristics and Identification, School of Information Science and Engineering, Southeast University, Nanjing, P.R. China.

^{††}The author is with the School of Electronics and Information Engineering, Soochow University, Suzhou, P.R. China.

a) E-mail: tjcui@seu.edu.cn

DOI: 10.1587/transcom.E94.B.1142

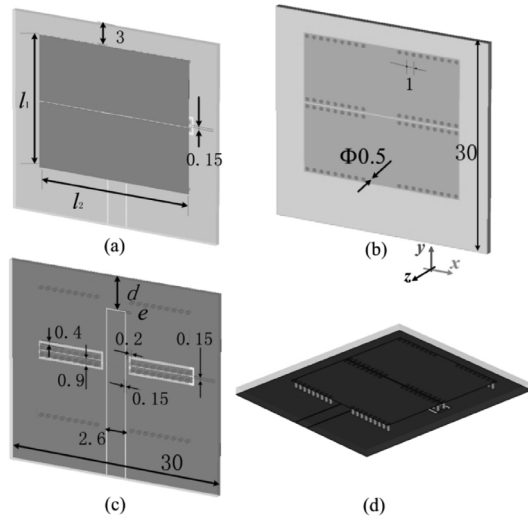


Fig. 1 The geometry of the SRR-based antenna. (a) Top surface. (b) Mid-layer. (c) Bottom surface. (d) The overall topology of the antenna (Unit: mm).

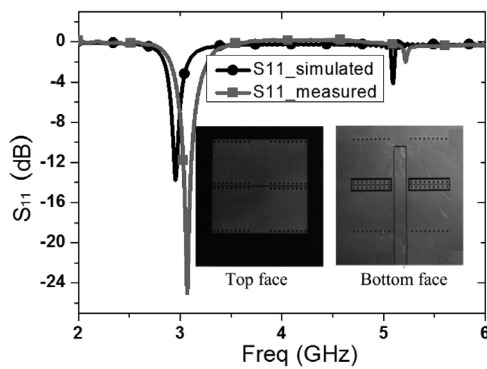


Fig. 2 The simulated and measured S_{11} parameters of the SRR-based antenna structure.

tion patches due to the existence of the CPW ground plane. The dimension of the radiation patches are $l_1 = 20$ mm, $l_2 = 22$ mm, the gap between them is 0.15 mm, and the distance from the end of radiation patch to the edge of substrate is 5 mm, as shown in Fig. 1(a) [31]. The distance between the two adjacent vias is 0.5 mm with the diameter of 0.5 mm, as shown in Fig. 1(b). The gap between the CPW feed line and ground plane is 0.15 mm and the width of feed line is 2.6 mm to achieve the port impedance of 50Ω , as demonstrated in Fig. 1(c). The distance from the end of feed line to the edge of ground plane has a dramatic influence on the total magnetic flux in the antenna system, which determines the return loss of the antenna. This distance is optimized as $d = 9$ mm to provide the sufficient magnetic flux for the antenna. The open-ended CPW feed line is adopted in this design with $e = 0.2$ mm. The substrate is a standard F4B material with relative permittivity of 2.65. The thickness of substrate is 0.8 mm and the deposited copper thickness is 0.018 mm. The ground plane is square shaped in the plane with the size of $30\text{ mm} \times 30\text{ mm}$ [31].

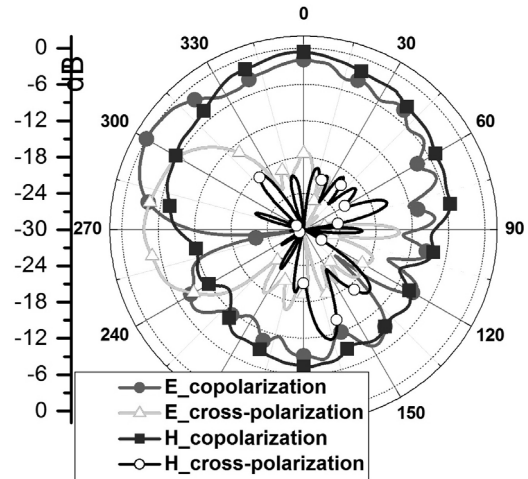


Fig. 3 The Measured Normalized radiation pattern of the improved SRR-based antenna.

Figure 2 shows that the measured resonant frequency of the antenna is 3.05 GHz, where the electrical size of the antenna is $0.204\lambda \times 0.224\lambda \times 0.0081\lambda$ [31]. The measured antenna gain is 2.25 dB at resonance and the corresponding measured normalized radiation pattern is shown in Fig. 3 [31]. The cross-polarization level in the main lobe direction is about 20 dB lower than the co-polarization in both E and H planes and the front-to-back ratio is relatively good (7.5 dB). Comparatively, conventional patch antenna with the same resonant frequency and the same dimensions as the SRR-based antenna (such conditions could be satisfied by setting the relative permittivity of patch antenna as 6.11) has a lower radiation efficiency (69%) than the above SRR-based antenna (88%).

3. Metamaterial-Substrate Patch Antennas [39]

Conventional patch antennas suffer from narrow impedance bandwidth. One of the approaches to improve its bandwidth without increasing antenna size and height (or volume) is to utilize magneto-dielectric substrate with enhanced magnetic response which lowers the quality factor of the patch antenna [40], [41]. In the past a few years, some efforts have been conducted to make use of artificial magneto-dielectric substrates in patch antennas. Such artificial magneto-dielectric materials are usually composed of metal structures with magnetic responses (e.g. SRRs), which are easily realized in the microwave frequencies with low loss. When the artificial magneto-dielectric materials are loaded into patch antennas, they are usually stacked between the ground plane and antenna patch [42]–[44].

Figure 4 shows the microstrip patch antenna loaded with a compact artificial magneto-dielectric substrate [39]. This antenna requires simple single-layer PCB techniques for fabrication and consists of a supporting dielectric, a radiating patch and a ground plane on two sides of the dielectric, separately. It has additional etched patterns right under the patch in the ground metallization compared to the conven-

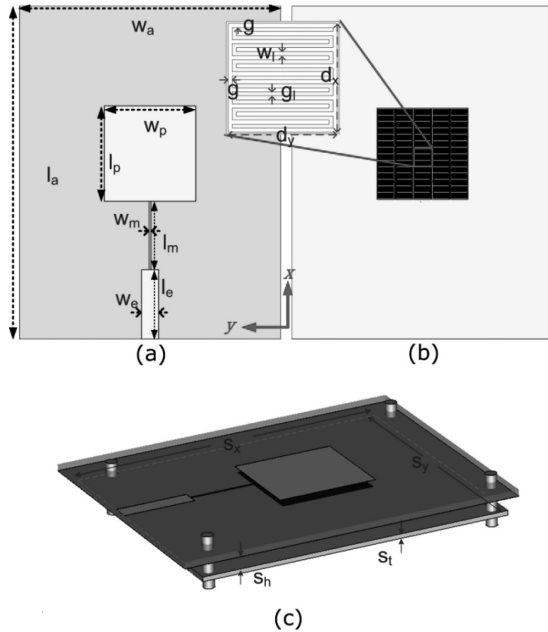


Fig. 4 The illustration of microstrip antenna loaded with waveguided magneto-dielectric metamaterial of EML array. The yellow area indicates metallization and the green area indicates the supporting dielectric. (a) Front view. (b) Back view. (c) EML-based antenna with an additional shield metal plate.

tional patch antenna. The etched patterns is a periodically arranged array with 5 identical planar unit cells along each of the two orthogonal directions in the ground plane. The planar unit cell characterizes a meander line embedded in a square area defect in the ground and hence is called as embedded meander-line (EML) [39]. The EML periodicity is 4.2 mm along each direction and the EML geometries are $d_x = 4.05$ mm, $d_y = 4.05$ mm, $g = 0.15$ mm, $g_l = 0.15$ mm, and $w_l = 0.15$ mm. The thickness, permittivity and loss tangent of the supporting dielectric are $h = 1.43$ mm, 2.65 and 0.001, respectively. The EML array together with the supporting dielectric and the top metallization (i.e. the metallic patch) constitute a kind of waveguided metamaterial [45]–[47] with effective magneto-dielectric properties, acting as the artificial substrate of the antenna. The effective medium parameters μ_y and ϵ_z of the EML-based waveguided metamaterial are shown in Fig. 5 [39]. It can be seen that the EML-based waveguided metamaterial has a lowered permittivity with respect to the supporting dielectric and an enhanced permeability with weak dispersion before resonance. Around the antenna working frequency (about 3.5 GHz), the effective medium parameters are $\epsilon_z \approx 1.83 - j0.0077$ and $\mu_y \approx 2.22 - j0.0427$.

The antenna patch width and patch length are $w_p = 21$ mm and $l_p = 22$ mm [39]. The dimensions of the feeding network are: $w_e = 3.86$ mm, $l_e = 16$ mm, $w_m = 0.42$ mm, and $l_m = 15.34$ mm, where w_e and l_e are the width and length of 50 Ohm microstrip feeding line, respectively, and w_m and l_m are the width and length of the quarter-wavelength matching line, respectively, as shown in Fig. 4(a). The

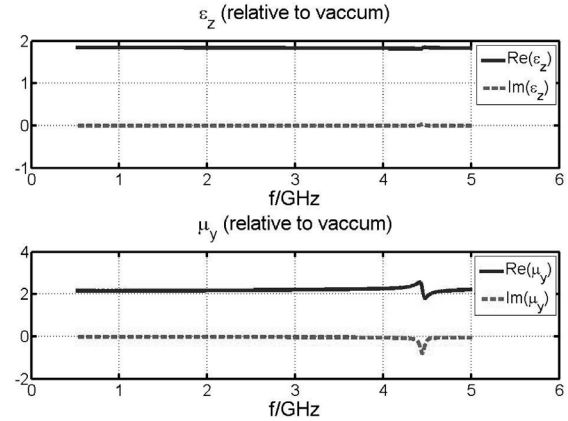


Fig. 5 The effective medium parameters of the EML-based waveguided metamaterial.

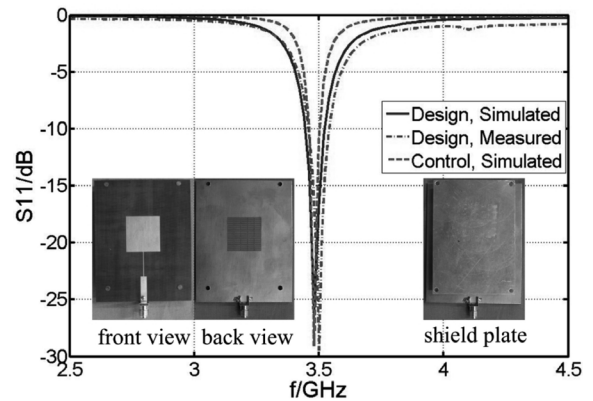


Fig. 6 The simulated and measured reflection coefficient of the EML-based patch antenna (solid line and dash dot line, respectively) and the simulated reflection coefficient of the control antenna (dashed line).

overall sizes of the resulting antenna are 60 mm wide and 76.34 mm long. To suppress the back radiation due to the defects in the ground plane, an additional metal shield plate is added beneath and parallel to the antenna ground, as shown in Fig. 4(c). The sizes of shield plate are $s_x = 70$ mm, $s_y = 50$ mm, $s_t = 1$ mm, and the distance between the shield and antenna ground is $s_h = 5$ mm. According to Ref. [40], the bandwidth improvement factor of the EML-based patch antenna over control antenna could be estimated as 2.06 by the following expression

$$\text{BIF} = \sqrt{\epsilon_d \mu_y / \epsilon_z}, \quad (1)$$

where $\epsilon_d = 3.51$ is the substrate permittivity of the control antenna. We remark that the control antenna is a conventional patch antenna based on purely dielectric substrate. It has the same overall size, the same patch size and the same supporting dielectric thickness as the EML-based antenna. Both antennas have nearly the same working frequency.

The reflection coefficients of the EML-based patch antenna and the control antenna are given in Fig. 6 [39], where the fabricated EML-based antenna is shown in the inset. The simulated and measured -10 dB bandwidths of the EML-

based antenna are 77.7 MHz and 76 MHz, while the simulated -10 dB bandwidth of the control antenna is 42 MHz. Clearly, the bandwidth improvement factor is about 1.85, which is close to the theoretical prediction. Figure 7 compares the simulated magnetic field distribution under the patch at resonance for the EML-based antenna and the control antenna [39]. It is obvious that the magnetic-field intensity (and hence the stored energy) of the EML-based antenna is much smaller than that of the control antenna, indicating that the quality factor of antenna is decreased by using the artificial magneto-dielectric loading. The EML loading together with metal shield plate has little influence on the radiation characteristic (radiation efficiency, forward co-polarization gain etc.) of the patch antenna. The measured E-plane and H-plane radiation patterns of the EML-based antenna at the central working frequency 3.494 GHz are shown in Fig. 8 [39], which reveals that front-to-back ratios in E and H planes are 11.98 dB and 20.76 dB, re-

spectively, and the cross-polarizations in E and H planes are about -21.07 dB and -19.58 dB, respectively.

4. Metamaterial Flat-Lens Antennas [48]

Lens antenna is widely used in microwave frequency due to its high directivity and wide bandwidth. It is designed to transform the spherical wave front, which is emitted from a feed at the focus, into planar wave front. The classic microwave lens is composed of homogeneous dielectric material with curvilinear shape. However, inhomogeneous index distribution could bring additional benefit such as the flat surface and large scanning angle to lens antenna [49], [50]. This can be conveniently achieved by metamaterials whose particles could be tuned independently [51]. Alternatively, flat lens antennas could also be realized using negatively-graded refractive index [52], which may suffer from the loss and the frequency bandwidth.

Impedance matching with free space is an important issue for the flat GRIN lens antenna [48]. By utilizing metamaterials whose effective wave impedance is close to that of free space to construct the GRIN lens, good impedance matching could be achieved without designing matching layers. This is an advantage over the conventional GRIN lens composed of pure dielectric materials.

Figure 9 shows a sample of two-dimensional (2D) beam-scanning GRIN lens antennas realized by metamaterials, whose unit cell is given in the right-lower corner of

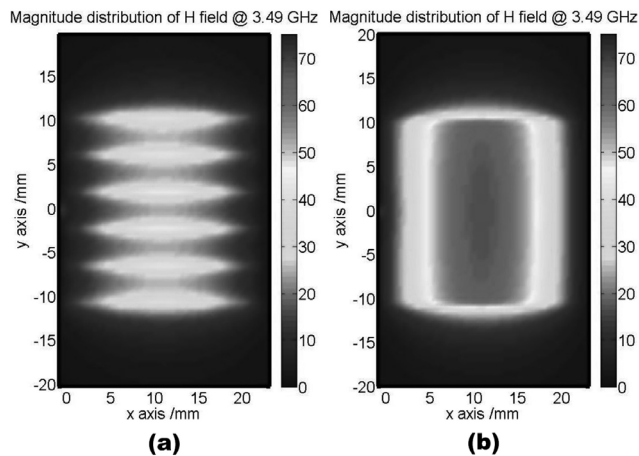


Fig. 7 The simulated magnetic-field intensity distribution under the patch at the resonance. (a) The antenna with the EML array. (b) The control antenna.

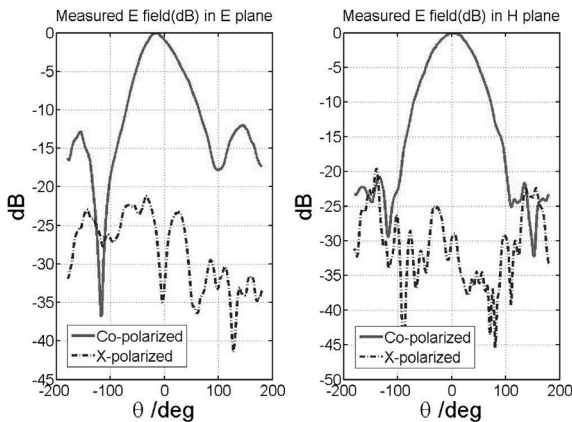


Fig. 8 The measured radiation pattern of the patch antenna with the EML array at 3.494 GHz. In the E plane, the positive/negative θ value corresponds to the $\phi = 0^\circ/\phi = 180^\circ$ half plane. In the H plane, the positive/negative θ value corresponds to the $\phi = 90^\circ/\phi = 270^\circ$ half plane.

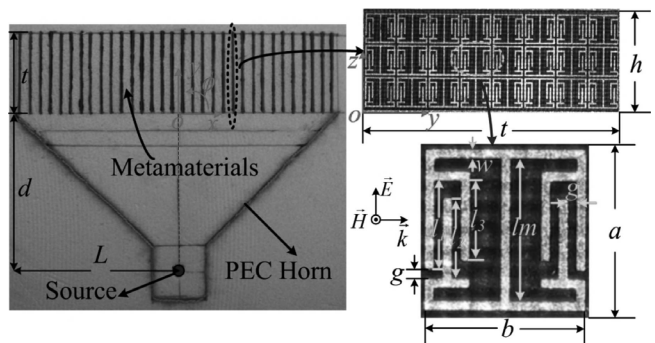


Fig. 9 The experiment sample of beam-scanning metamaterial lens antenna and the involved metamaterial unit cell.

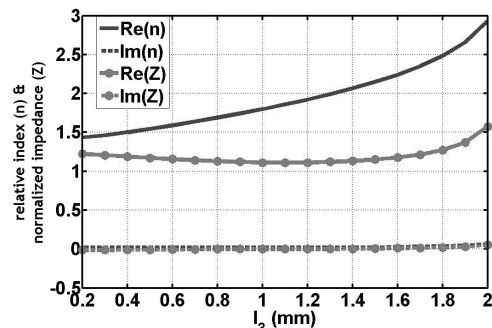


Fig. 10 The effective index of refraction (n) and wave impedance (Z) of metamaterial unit cells with varied l_3 at 8 GHz (l_2 is fixed as 1.8 mm).

Fig. 9 [48]. A line source is located on the central axis of the lens with a distance of $d = 60$ mm to excite the lens. A perfectly electrical conducting (PEC) horn is placed behind the source to restrain the back radiation. The metamaterial lens is $2L = 121.6$ mm long and $t = 30.4$ mm thick. The height of the lens h is finite (12 mm) for the sake of near-field measurement. It is equally divided into 32 pieces of printed circuit boards (PCBs) and each PCB contains 8 unit cells along the optical axis. The metamaterial unit cell here is a subwavelength resonator loaded with two interdigital capacitors and adheres to the F4B substrate whose thickness is 0.5 mm and permittivity is 2.65 with loss tangent 0.001. Since the incident waves propagate along the y direction with the electric-field polarized along the z -direction (see Fig. 9), electric and magnetic responses can be inspired simultaneously for the unit cell to achieve effective wave impedance close to unity. The periodicity and dimensions of the unit cell are $a = 3.8$ mm, $b = 3.6$ mm, $w = 0.2$ mm, $g = 0.2$ mm, $l_1 = 2$ mm and $lm = 3.2$ mm. The digit lengths l_2 and l_3 in the interdigital capacitor are adjusted to satisfy the inhomogeneous index distribution along the x direction as [48]

$$n(x) = n_0 - [x \sin \theta + (\sqrt{d^2 + x^2} - d)]/t, \quad (2)$$

where n_0 is the index of refraction at $x = 0$. The GRIN lens with such a index distribution approximately transforms the quasi-cylindrical wave excited by a line source to the plane wave at a deflection angle θ with respect to the y axis. Three

cases of deflection angles $\theta = 0^\circ$, $\theta = 15^\circ$, and $\theta = 30^\circ$ were considered for the metamaterial lenses at 8 GHz [48]. These cases correspond to initial index of $n_0 = 1.8$, $n_0 = 2.3$, and $n_0 = 2.4$, respectively. The total index range required by the three case is from 1.05 to 2.8, which is divided into two regions: [1.34,2.8] and [1.05,1.29]. The first index range is achieved by fixing l_2 as 1.8 mm and tuning l_3 from 0.2 mm to 2 mm; while the second index range is achieved by fixing l_2 as 1.5 mm and tuning l_3 from 0.8 mm to 1.1 mm. The effective impedances obtained through this manner have a good match to that of free space. Figure 10 illustrates the effective medium response of the unit cell when l_2 is fixed as 1.8 mm and l_3 changes from 0.2 mm to 2 mm at 8 GHz [48].

The near-field distributions of the three metamaterial flat lens antennas with different beam deflection angles have been measured using the 2D near-field measurement apparatus (2D Mapper) [53] and are illustrated in Figs. 11(a), (b) and (c) [48]. Nearly no reflections can be observed from these results, which validate the design of the antennas. The simulated and measured far-field radiation patterns with 0-degree beam deflection at 8 GHz, which are in good agreements, are shown in Fig. 11(d). They exhibit good directive behaviors and low sidelobes (below -18 dB).

5. Metamaterial Luneberg-Lens Antenna [54]

The Luneberg lens antennas [55] have been widely used in mobile satellite communications. It transforms the spherical waves from a point source on its surface into plane waves on the diametrically opposite side of the lens. The 2D Luneberg lens has a circular symmetry with the refractive index varying from 1 to $\sqrt{2}$ with the rule of $n = \sqrt{2 - (r/R)^2}$, where R is the radius of the Luneberg lens and $0 \leq r \leq R$.

Recently, several work has been reported on Luneberg lens antennas which were realized by metamaterials [54], [56], [57]. Besides the traditional Luneberg lens [54], the transformation optics [58] has been used to produce flattened Luneberg lenses which possess planar focal plane and zero focal distance [56], [57]. Here, we only introduce the traditional Luneberg lens realized by metamaterials.

Figure 12 shows a 2D metamaterial Luneberg lens designed at the frequency $f = 8$ GHz with a radius of $R = 49.4$ mm and a finite height of 12 mm for the sake of near-field measurement [54]. The metamaterial Luneberg lens consists of 1548 planar I-shaped metallic unit cells [10] separately printed on 24 thin dielectric boards with permittivity of 2.65. The I-shaped structure is shown in Fig. 12(d). The dielectric and copper thickness of those PCB boards are 0.25 mm and 0.018 mm, respectively. They are embedded in an air-like foam and have different lengths to approximate the circular shape of the lens. The continuous index distribution of the lens is discretized by a set of rectangular grids in accordance with the separate PCB boards, as shown in Fig. 12(a), resulting a discrete refractive-index distribution for the Luneberg lens, as shown in Fig. 12(b). The geometrical parameter g of the I-shaped unit cell varies spatially

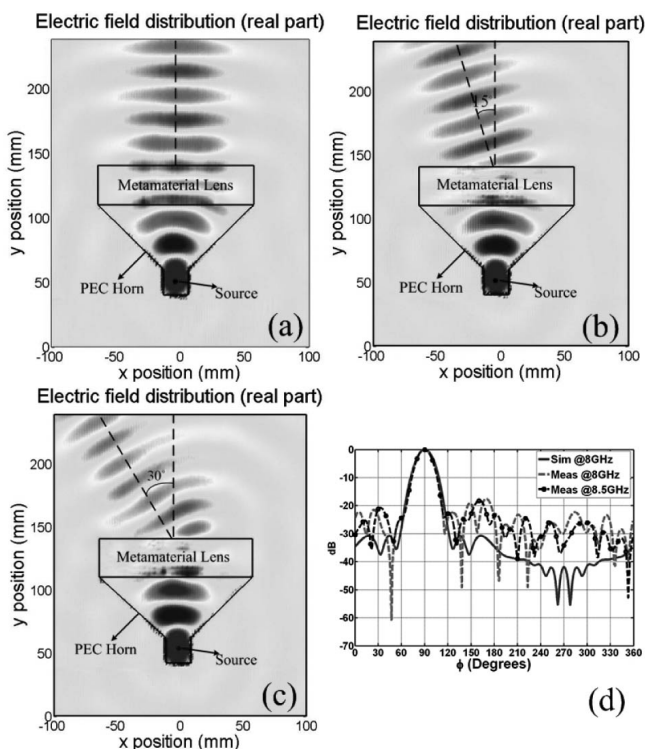


Fig. 11 The measured results for beam-scanning metamaterial lens antennas. (a)-(c) Near-field distributions for 0, 15, 30-degree beam deflections. (d) Far-field radiation patterns for 0-degree beam deflection.

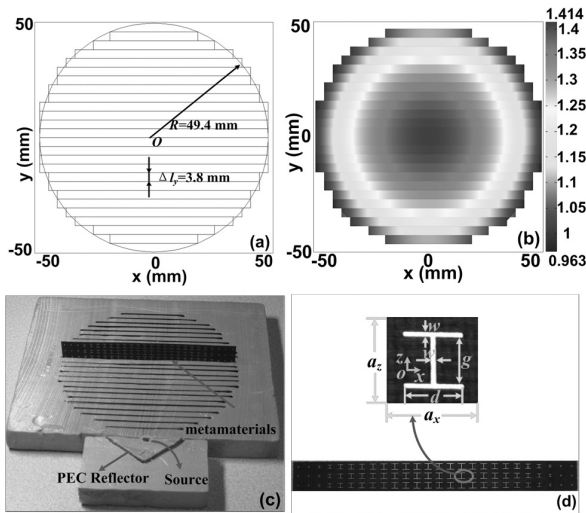


Fig. 12 The design of metamaterial Luneberg lens antenna. (a) The discrete rectangular grid approximating a circular Luneberg Lens, (b) The relative refractive index distributions, (c) The experimental sample of the lens, (d) The details of the metamaterials in (c).

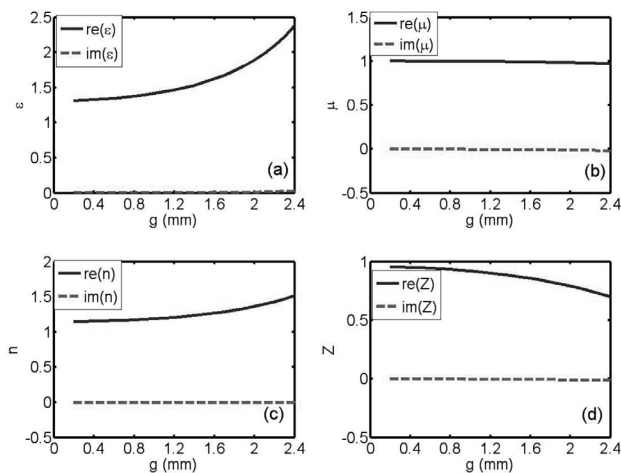


Fig. 13 The relationship between the geometry g and the effective medium parameters of the I-shaped structure.

throughout the lens to realize the discrete index distribution. The periodicity and other geometrical parameters of all I-shaped unit cells are $a_x = a_z = 3.8$ mm, $w = 0.2$ mm, and $d = g + 2w$ [54]. Note that the minimum n available with the I-shaped unit cell is 1.15, hence the discrete indexes smaller than 1.15 are all designed as 1.15. The effective permittivity ϵ_r increases monotonously as g increases, and the relative permeability μ_r is very close to unity for the I-shaped structure, as shown in Fig. 13 [54]. Besides, the effective medium parameters of I-shaped structure nearly remain the same within the frequency band from 7 GHz to 9 GHz. Compared to the traditional Luneberg lens, the above novel metamaterial Luneberg lens is easier to fabricate with lower price and lighter weight.

The near-field distributions of the 2D metamaterial Luneberg lens antenna were measured using the 2D map-

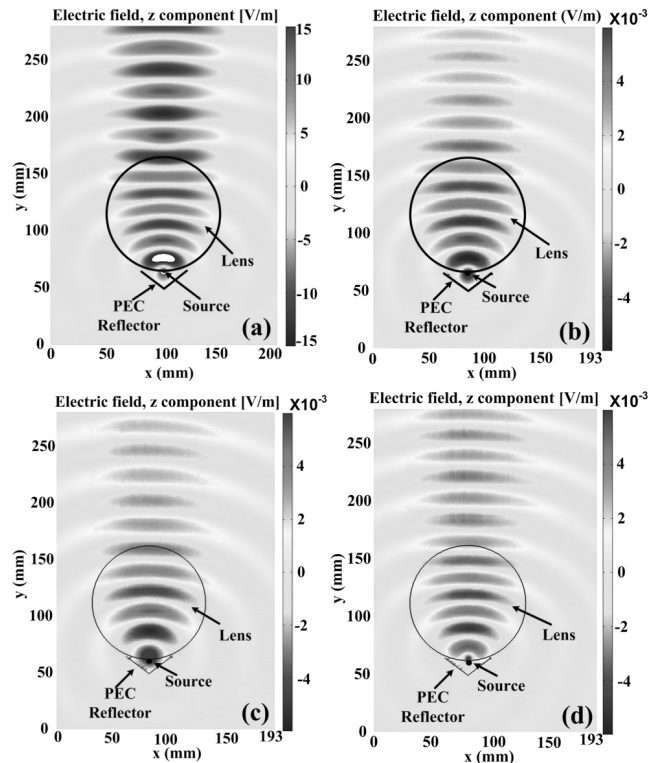


Fig. 14 The electric field distributions of the metamaterial Luneberg lens antenna, (a) The simulated result at 8 GHz, (b) The measured result at 8 GHz, (c) The measured result at 7 GHz, (d) The measured result at 8.5 GHz.

per [54], and were transformed to the far-field radiation patterns using the near-far field transformation technology [59]. In the experiment, a conducting reflector is placed against the metamaterials lens to restrain the back radiation of the line source used to feed the lens, as shown in Fig. 12(c). The experimental results have good agreements to the simulation results, as shown in Figs. 14(a), 14(b) and 15(a) [54]. Considering the relatively small electric-size aperture ($2R = 2.63\lambda$), the metamaterial lens antenna has a good performance with relatively high gain. Figures 14(c) and (d) give the measured near-field distributions at 7 GHz and 8.5 GHz, and Fig. 15(b) gives the measured radiation patterns at 7 GHz, 8 GHz and 8.5 GHz, demonstrating that the metamaterial lens antenna works well in a wide frequency band.

6. Conformal Lens Antennas Made of Anisotropic Zero-Index Metamaterials

Recently, due to the potential to enhance the directivity of antennas, zero refractive index metamaterials (ZIMs) have aroused great interest [60], [61]. We have shown that a feeding monopole embedded in an anisotropic ZIM directly radiates plane waves instead of spherical waves, when one component of the permeability tensor approaches zero [61]. Based on such a property, a highly directive emission of electromagnetic waves can be obtained based on the

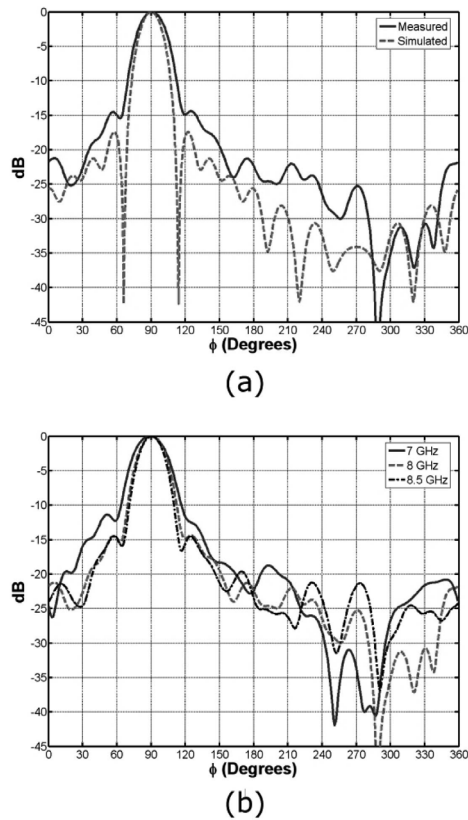


Fig. 15 The far-field radiation patterns of the metamaterial Luneberg-like lens antenna. (a) The simulated and measured results at 8 GHz. (b) The measured results at 7 GHz, 8 GHz, and 8.5 GHz.

anisotropic ZIM with arbitrary shapes. It should be noted that the wave impedance of air and anisotropic metamaterial could be designed as matching, to make high-efficiency emission.

In this section, we propose a kind of novel conformal antennas using the anisotropic ZIMs, which can be attached to arbitrarily-shaped PEC object. In the following designs, the electromagnetic parameters of the anisotropic metamaterials are chosen as $\mu_x = 1$, $\mu_y = 10^{-5}$, and $\epsilon_z = 1$. We have designed the anisotropic metamaterial in the X band (10 GHz), and observed their highly directive emission from both near-field distributions and far-field radiations.

We first consider a small-sized anisotropic ZIM antenna (4-wavelength aperture) covered on a planar PEC patch. The feeding monopole is embedded in the anisotropic metamaterial. Even in the small-aperture case, the plane-wave feature is well conserved in the near-field region outside the metamaterial, and the waves can be emitted to the far-field region as a highly directive beam. This can be clearly observed from the simulation result demonstrated in Fig. 16(a). Since the wave impedance in the anisotropic metamaterial is matched to that in free space, the plane waves will be emitted without any reflections in the forward direction. As a comparison, the near-field distribution of a GRIN lens antenna with the same aperture is given in Fig. 16(b). Clearly, the anisotropic ZIM antenna has a bet-

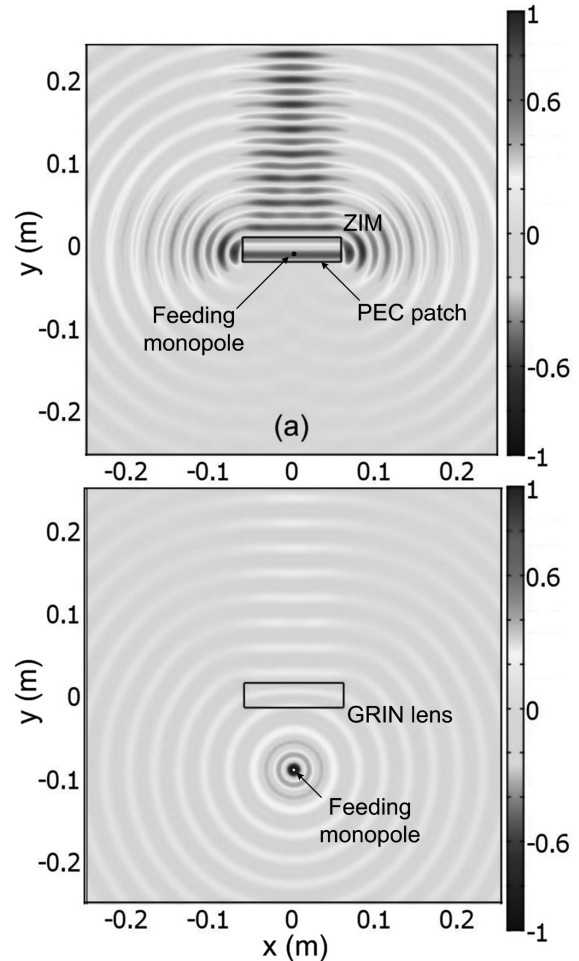


Fig. 16 (a) The near-field distribution of the anisotropic ZIM antenna. (b) The near-field distribution of the GRIN antenna. The aperture of both antennas is 12mm (4 wavelengths).

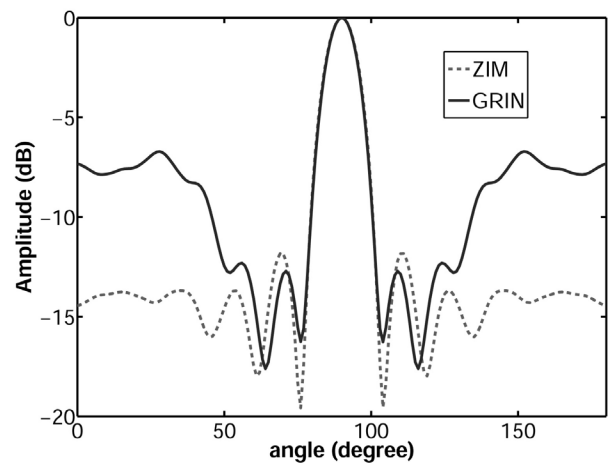


Fig. 17 The comparison of normalized radiation patterns of the ZIM and GRIN antennas with 4-wavelength aperture.

ter performance than the GRIN lens to generate high-quality plane waves. The comparison of far-field radiation patterns of the two antennas is shown in Fig. 17. We clearly observe

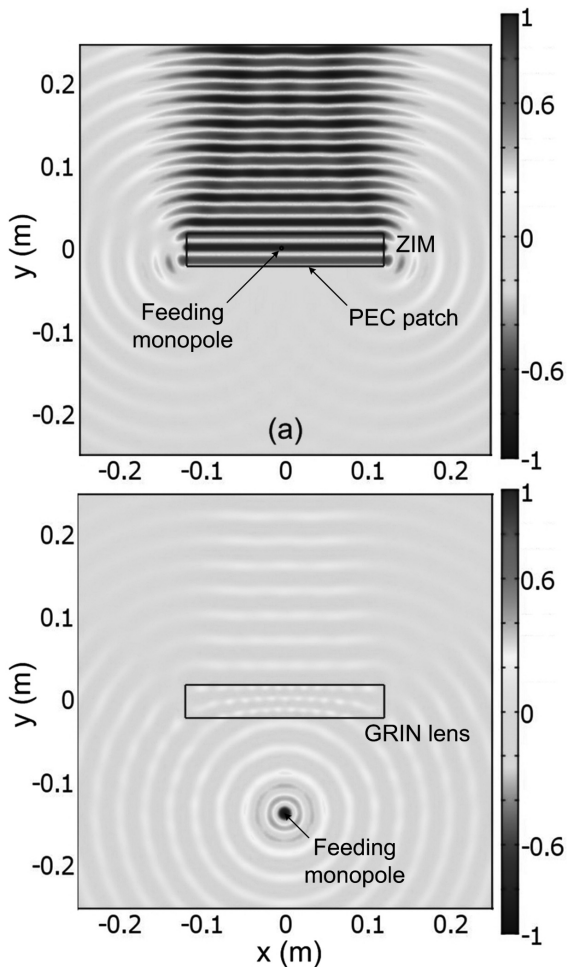


Fig. 18 (a) The near-field distribution of the anisotropic ZIM antenna. (b) The near-field distribution of the GRIN antenna. The aperture of both antennas is 24mm (8 wavelengths).

that the anisotropic ZIM antenna has a higher directivity and lower sidelobes than the GRIN lens. When the aperture sizes of both antennas are increased to 8 wavelengths, the near-field distributions are illustrated in Fig. 18 and the far-field radiation patterns are shown in Fig. 19, further confirming the above conclusions.

In real applications, conformal antennas are usually required. In another word, the antennas are always designed to have conformal shapes to the surface of the mechanical carrier (such as the head of an aircraft). It is expected that the properties of the conformal antennas are similar to those of planar antennas, regardless of the boundary shape. In the earlier design, the anisotropic ZIM is shaped to a flat PEC patch, which shows excellent directivity under the excitation of a monopole antenna. Next we consider another example, in which the anisotropic ZIM is designed on a semicircular PEC object, and the outer boundary-shape is also semicircular, as shown in Fig. 20. The simulation results are demonstrated in Fig. 20, where the monopole antenna is also embedded in the anisotropic metamaterial. Two cases are considered, in which the outer radius of ZIM antenna is fixed

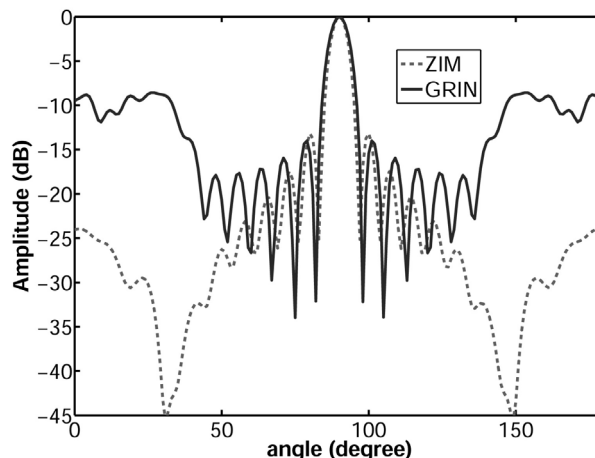


Fig. 19 The comparison of normalized radiation patterns of the ZIM and GRIN antennas with 8-wavelength aperture.

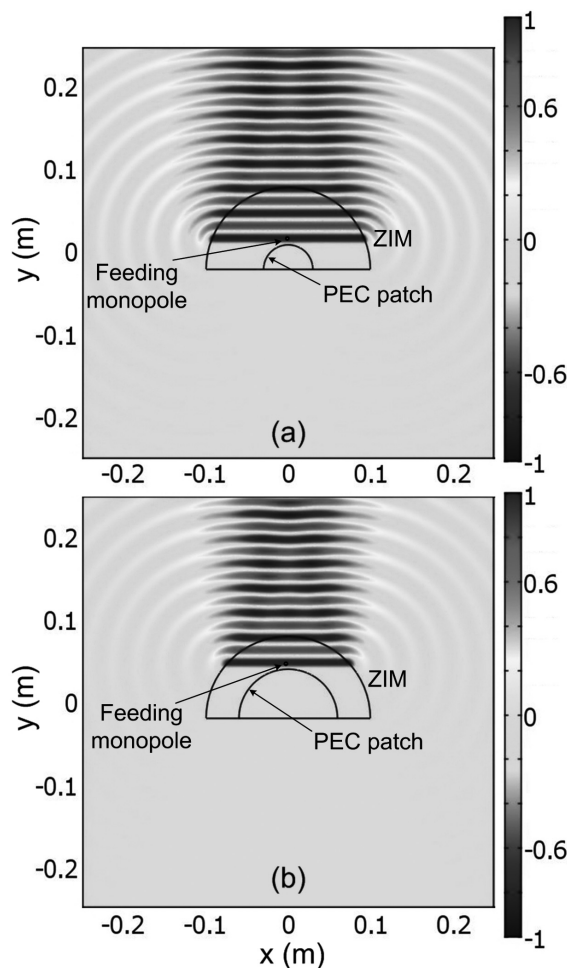


Fig. 20 The near-field distributions of the semi-circular conformal ZIM antennas. The outer radius of the antenna is 100 mm. (a) The inner radius of the antenna $r_0 = 30$ mm. (b) The inner radius of the antenna $r_0 = 60$ mm.

to 100 mm. In the first case, the inner radius of the antenna (or the radius of the PEC object) is 30 mm (see Fig. 20(a)), hence the antenna has a large volume and the object has a

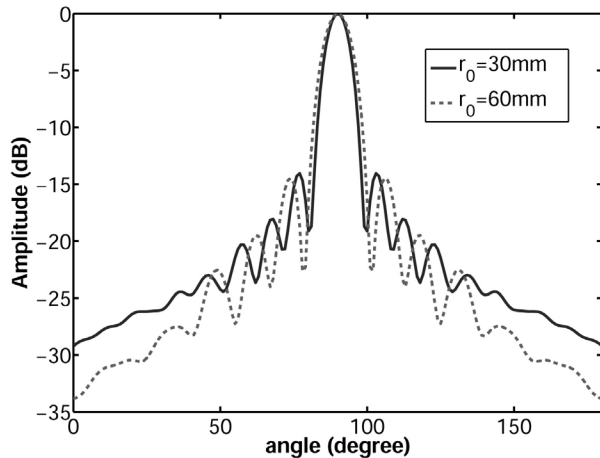


Fig. 21 The normalized radiation patterns of the conformal antennas with different inner radii.

small size. In the second case, the inner radius (or the radius of the object) is 60 mm (see Fig. 20(b)), and hence the antenna has a small volume and the object has a large size. In both cases, very good directivities are observed. From the near-field distributions shown in Fig. 20, we notice that the plane waves are generated inside the semicircular metamaterial, and then, the waves are emitted at the curved interface. We clearly see that the near-field patterns are insensitive to the shape variance of the metamaterial. The plane waves are always directed to the y direction, the anisotropic direction. The far-field radiation patterns of both cases are illustrated in Fig. 21, in which high directivities and low sidelobes have been verified.

7. Conclusions

Several applications of metamaterials on microwave antennas have been presented. Resonant metamaterial unit cells with sub-wavelength are suitable in designing electrically-small antennas. By utilizing waveguided magneto-dielectric metamaterial as the substrate of patch antenna, the impedance bandwidth of patch antenna can be improved with little influences on the radiation characteristic. Non-resonant metamaterials could be used to construct GRIN lens with broadband beam-steering performance. Conformal lens antennas with good impedance matching and high-efficiency emission could be achieved using anisotropic zero-index metamaterials. All such applications confirm that metamaterials provide promising approach in the future antenna engineering.

References

- [1] V.G. Veselago, "The electrodynamics of substances with simultaneously negative values of ϵ and μ ," *Sov. Phys. Usp.*, vol.3, pp.509–514, 1968.
- [2] T.J. Cui, D.R. Smith, and R. Liu, eds., *Metamaterials—Theory, Design, and Applications*, Springer, 2009.
- [3] J.B. Pendry, D. Schurig, and D.R. Smith, "Controlling electromagnetic fields," *Science*, vol.312, pp.1780–1782, 2006.

- [4] D. Schurig, J.J. Mock, B.J. Justice, S.A. Cummer, J.B. Pendry, A.F. Starr, and D.R. Smith, "Metamaterial electromagnetic cloak at microwave frequencies," *Science*, vol.314, pp.977–980, 2006.
- [5] U. Leonhardt, "Optical conformal mapping," *Science*, vol.312, pp.1777–1780, 2006.
- [6] S.A. Cummer, B.-I. Popa, D. Schurig, D.R. Smith, and J.B. Pendry, "Full-wave simulations of electromagnetic cloaking structures," *Phys. Rev. E*, vol.74, 036621, 2006.
- [7] W. Cai, U.K. Chettiar, A.V. Kildishev, and V.M. Shalaev, "Optical cloaking with metamaterials," *Nat. Photon.*, vol.1, pp.224–227, 2007.
- [8] W.X. Jiang, J.Y. Chin, Z. Li, Q. Cheng, R. Liu, and T.J. Cui, "Analytical design of conformally invisible cloaks for arbitrarily shaped objects," *Phys. Rev. E*, vol.77, 066607, 2008.
- [9] J. Li and J.B. Pendry, "Hiding under the carpet: A new strategy for cloaking," *Phys. Rev. Lett.*, vol.101, 203901, 2008.
- [10] R. Liu, C. Ji, J.J. Mock, J.Y. Chin, T.J. Cui, and D.R. Smith, "Broadband ground-plane cloak," *Science*, vol.323, pp.366–369, 2009.
- [11] J. Valentine, J. Li, T. Zentgraf, G. Bartal, and X. Zhang, "An optical cloak made of dielectrics," *Nat. Mater.*, vol.8, pp.568–571, 2009.
- [12] L.H. Gabrielli, J. Cardenas, C.B. Poitras, and M. Lipson, "Silicon nanostructure cloak operating at optical frequencies," *Nat. Photo.*, vol.3, pp.461–463, 2009.
- [13] H.F. Ma and T.J. Cui, "Three-dimensional broadband ground-plane cloak made of metamaterials," *Nat. Comm.*, DOI, 10.1038/ncomms1023, 2009.
- [14] M. Rahm, D. Schurig, D.A. Roberts, S.A. Cummer, D.R. Smith, and J.B. Pendry, "Design of electromagnetic cloaks and concentrators using form-invariant coordinate transformations of Maxwell's equations," *Photon. Nano.- Fund. Appl.*, vol.6, pp.87–95, 2008.
- [15] W.X. Jiang, T.J. Cui, Q. Cheng, J.Y. Chin, X.M. Yang, R. Liu, and D.R. Smith, "Design of arbitrarily shaped concentrators based on conformally optical transformation of nonuniform rational B-spline surfaces," *Appl. Phys. Lett.*, vol.92, 264101, 2008.
- [16] H. Chen and C.T. Chan, "Transformation media that rotate electromagnetic fields," *Appl. Phys. Lett.*, vol.90, 241105, 2007.
- [17] Y. Luo, J. Zhang, B.-I. Wu, and H. Chen, "Interaction of an electromagnetic wave with a cone-shaped invisibility cloak and polarization rotator," *Phys. Rev. B*, vol.78, 125108, 2008.
- [18] J.Y. Chin, M.Z. Lu, and T.J. Cui, "Metamaterial polarizers by electric-field-coupled resonators," *Appl. Phys. Lett.*, vol.93, no.25, 251903, 2008.
- [19] J.M. Hao, Y. Yuan, L.X. Ran, T. Jiang, J.A. Kong, C.T. Chan, and L. Zhou, "Manipulating electromagnetic wave polarizations by anisotropic metamaterials," *Phys. Rev. Lett.*, vol.99, no.6, 063908, 2007.
- [20] F. Kong, B. Wu, J.A. Kong, J. Huangfu, S. Xi, and H. Chen, "Planar focusing antenna design by using coordinate transformation technology," *Appl. Phys. Lett.*, vol.91, 253509, 2007.
- [21] W.X. Jiang, T.J. Cui, H.F. Ma, X.M. Yang, and Q. Cheng, "Layered high-gain lens antennas via discrete optical transformation," *Appl. Phys. Lett.*, vol.93, 221906, 2008.
- [22] Y. Luo, J. Zhang, H. Chen, J. Huangfu, and L. Ran, "High-directivity antenna with small antenna aperture," *Appl. Phys. Lett.*, vol.95, 193506, 2009.
- [23] J. Zhang, Y. Luo, S. Xi, H. Chen, L. Ran, B.-I. Wu, and J.A. Kong, "Directive emission obtained by coordinate transformation," *Prog. Electro. Resear.-PIER*, vol.81, pp.437–446, 2008.
- [24] W.X. Jiang, T.J. Cui, H.F. Ma, X.Y. Zhou, and Q. Cheng, "Cylindrical-to-plane-wave conversion via embedded optical transformation," *Appl. Phys. Lett.*, vol.92, 261903, 2008.
- [25] Y. Luo, J. Zhang, L. Ran, H. Chen, and J.A. Kong, "New concept conformal antennas utilizing metamaterial and transformation optics," *IEEE Antennas Wireless Propag. Lett.*, vol.7, pp.509–512, 2008.
- [26] N. Kundtz, D.A. Roberts, J. Allen, S. Cummer, and D.R. Smith, "Optical source transformations," *Opt. Express*, vol.16, no.26,

- pp.21215–21222, 2008.
- [27] Y. Lai, J. Ng, H. Chen, D. Han, J. Xiao, Z.-Q. Zhang, and C.T. Chan, “Illusion optics: The optical transformation of an object into another object,” *Phys. Rev. Lett.*, vol.102, 253902, 2009.
- [28] W.X. Jiang, H.F. Ma, Q. Cheng, and T.J. Cui, “Illusion media: Generating virtual objects using realizable metamaterials,” *Appl. Phys. Lett.*, vol.96, 121910, 2010.
- [29] W.X. Jiang and T.J. Cui, “Moving targets virtually via composite optical transformation,” *Opt. Express*, vol.18, pp.5161–5167, 2010.
- [30] W.X. Jiang, H.F. Ma, Q. Cheng, and T.J. Cui, “Virtual conversion from metal object to dielectric object using metamaterials,” *Opt. Express*, vol.18, pp.11276–11281, 2010.
- [31] M. Li, X.Q. Lin, J.Y. Chin, R. Liu, and T.J. Cui, “A novel miniaturized printed planar antenna using split-ring resonator,” *IEEE Antennas and Wireless Propagation Letters*, vol.7, pp.629–631, 2008.
- [32] H. Mosallaei and K. Sarabandi, “Magneto-dielectrics in electromagnetics: Concept and applications,” *IEEE Trans. Antennas Propag.*, vol.52, no.6, pp.1558–1567, June 2004.
- [33] F. Qureshi, M.A. Antoniadis, and G.V. Eleftheriades, “A compact and low-profile metamaterial ring antenna with vertical polarization,” *IEEE Antennas Wireless Propag. Lett.*, vol.4, pp.333–336, 2005.
- [34] F. Bilotti, A. Alu, and L. Vegni, “Design of miniaturized metamaterial patch antennas with μ -negative loading,” *IEEE Trans. Antennas Propag.*, vol.56, no.6, pp.1640–1647, June 2008.
- [35] R.W. Ziolkowski and A. Erentok, “Metamaterial-based efficient electrically small antennas,” *IEEE Trans. Antennas Propag.*, vol.54, no.7, pp.2113–2130, July 2006.
- [36] A. Erentok and R.W. Ziolkowski, “Metamaterial-inspired efficient electrically small antennas,” *IEEE Trans. Antennas Propag.*, vol.56, no.3, pp.691–707, March 2008.
- [37] D. Deslandes and K. Wu, “Integrated microstrip and rectangular waveguide in planar form,” *IEEE Microw. Wireless Compon. Lett.*, vol.11, no.8, pp.68–70, Aug. 2002.
- [38] J.B. Pendry, A.J. Holden, D.J. Robbins, and W.J. Stewart, “Magnetism from conductors and enhanced nonlinear phenomena,” *IEEE Trans. Microw. Theory Tech.*, vol.47, no.11, pp.2075–2084, Nov. 1999.
- [39] X.M. Yang, Q.H. Sun, Q. Cheng, X.Y. Zhou, and T.J. Cui, “Increasing the bandwidth of microstrip patch antenna by loading compact artificial magneto-dielectrics,” *IEEE Trans. Antennas Propag.*, vol.59, no.2, pp.373–378, Feb. 2011.
- [40] R.C. Hansen and M. Burke, “Antenna with magneto-dielectrics,” *Microw. Opt. Technol. Lett.*, vol.26, no.2, pp.75–78, 2000.
- [41] P. Ikonen and S.A. Tretyakov, “On the advantages of magnetic materials in microstrip antenna miniaturization,” *Microw. Opt. Technol. Lett.*, vol.50, no.12, pp.3131–3134, 2008.
- [42] K. Buell, H. Mosallaei, and K. Sarabandi, “A Substrate for small patch antennas providing tunable miniaturization factors,” *IEEE Trans. Microw. Theory Tech.*, vol.54, no.1, pp.135–146, 2006.
- [43] H. Mosallaei and K. Sarabandi, “Design and modeling of patch antenna printed on magneto-dielectric embedded-circuit metasubstrate,” *IEEE Trans. Antennas Propag.*, vol.55, no.1, pp.45–52, 2007.
- [44] P.M.T. Ikonen, S.I. Maslovski, C.R. Simovski, and S.A. Tretyakov, “On artificial magnetodielectric loading for improving the impedance bandwidth properties of microstrip antennas,” *IEEE Trans. Antennas Propag.*, vol.54, no.6, pp.1654–1662, 2006.
- [45] R. Liu, Q. Cheng, T. Hand, J.J. Mock, T.J. Cui, S.A. Cummer, and D.R. Smith, “Experimental demonstration of electromagnetic tunneling through an epsilon-near-zero metamaterial at microwave frequencies,” *Phys. Rev. Lett.*, vol.100, no.2, 023903, 2008.
- [46] R. Liu, X.M. Yang, J.G. Gollub, J.J. Mock, T.J. Cui, and D.R. Smith, “Gradient index circuit by waveguided metamaterials,” *Appl. Phys. Lett.*, vol.94, no.7, 073506, 2009.
- [47] Q. Cheng, R. Liu, J.J. Mock, T.J. Cui, and D.R. Smith, “Partial focusing by indefinite complementary metamaterials,” *Phys. Rev. B*, vol.78, no.12, 121102(R), 2008.
- [48] H.F. Ma, X. Chen, H.S. Xu, X.M. Yang, W.X. Jiang, and T.J. Cui, “Experiments on high-performance beam scanning antennas made of gradient-index metamaterials,” *Appl. Phys. Lett.*, vol.95, no.9, 094107, 2009.
- [49] E.W. Marchand, *Gradient index optics*, Academic Press, New York, 1978.
- [50] D.T. Moore, “Gradient-index optics: A review,” *Appl. Opt.*, vol.19, no.7, pp.1035–1038, April 1980.
- [51] D.R. Smith, J.J. Mock, A.F. Starr, and D. Schurig, “Gradient index metamaterials,” *Phys. Rev. E.*, vol.71, 036609, 2005.
- [52] R.B. Gregor, C.G. Parazzoli, J.A. Nielsen, M.A. Thompson, M.H. Tanielian, and D.R. Smith, “Simulation and testing of a graded negative index of refraction lens,” *Appl. Phys. Lett.*, vol.87, 091114, 2005.
- [53] B.J. Justice, J.J. Mock, L. Guo, A. Degiron, D. Schurig, and D.R. Smith, “Spatial mapping of the internal and external electromagnetic fields of negative index metamaterials,” *Opt. Express*, vol.14, pp.8694–8705, 2006.
- [54] H.F. Ma, X. Chen, X.M. Yang, H.S. Xu, Q. Cheng, and T.J. Cui, “A broadband metamaterial cylindrical lens antenna,” *Chinese Science Bulletin*, vol.55, no.19, pp.2066–2070, 2010.
- [55] R.K. Luneberg, *Mathematical Theory of Optics*, Providence, Brown University Press, Rhode Island, 1944.
- [56] N. Kundtz and D.R. Smith, “Extreme-angle broadband metamaterial lens,” *Nat. Mater.*, vol.9, pp.129–132, 2010.
- [57] H.F. Ma and T.J. Cui, “Three-dimensional broadband and broad-angle transformation-optics lens,” *Nature Communications*, vol.1, Nov. 2010.
- [58] D. Schurig, “An aberration-free lens with zero f-number,” *New J. Phys.*, vol.19, pp.115034–115044, 2008.
- [59] H.F. Ma, T.J. Cui, X.M. Yang, W.X. Jiang, and Q. Cheng, “Far-field predictions of metamaterials from two-dimensional near-field measurement system,” *Terahertz Science and Technology*, vol.3, no.2, pp.74–84, 2010.
- [60] Y.G. Ma, P. Wang, X. Chen, and C.K. Ong, “Near-field plane-wave-like beam emitting antenna fabricated by anisotropic metamaterial,” *Appl. Phys. Lett.*, vol.94, 044107, 2009.
- [61] Q. Cheng, W.X. Jiang, and T.J. Cui, “Radiation of planar electromagnetic waves by a line source in anisotropic metamaterials,” *J. Phys. D, Appl. Phys.*, vol.43, 335406, 2010.



Tie Jun Cui was born in September 1965, in Hebei, China. He received the B.Sc., M.Sc., and Ph.D. degrees in electrical engineering from Xidian University, Xi'an, China, in 1987, 1990, and 1993, respectively. In March 1993, he joined the Department of Electromagnetic Engineering, Xidian University, and was promoted to an Associate Professor in November 1993. From 1995 to 1997 he was a Research Fellow with the Institut für Hochfrequenztechnik und Elektronik (IHE) at the University of Karlsruhe,

Germany. In July 1997, he joined the Center for Computational Electromagnetics, Department of Electrical and Computer Engineering, University of Illinois at Urbana-Champaign, first as a Postdoctoral Research Associate and then a Research Scientist. In September 2001, he became a Cheung-Kong Professor with the Department of Radio Engineering, Southeast University, Nanjing, P. R. China. Currently, he is the Associate Dean with the School of Information Science and Engineering, and the Associate Director of the State Key Laboratory of Millimeter Waves. Dr. Cui is a Co-Editor of the book *Metamaterials - Theory, Design, and Applications* (Springer, Nov. 2009), the author of six book chapters. He has published over 200 peer-review journal papers in *IEEE Transactions*, *Science*, *Nature Communications*, *Physical Review Letters*, *Materials Today*, *SMALL*, *Physical Review B & E*, *Applied Physics Letters*, *Optics Letters*, *Optics Express*, etc. His research interests include metamaterials, wave propagations, scattering, inverse scattering, landmine detection, geophysical subsurface sensing, fast algorithms, microwave and millimeter wave circuits and antennas simulations. Currently, he is a principal investigator of more than 10 national projects. Dr. Cui was awarded a Research Fellowship from the Alexander von Humboldt Foundation, Bonn, Germany, in 1995, received a Young Scientist Award from the International Union of Radio Science (URSI) in 1999, was awarded a Cheung Kong Professor under the Cheung Kong Scholar Program by the Ministry of Education, China, in 2001, and received the National Science Foundation of China for Distinguished Young Scholars in 2002. He received several Best Paper Awards from the National and International Conferences and Organizations. Dr. Cui is a senior member of IEEE and a member of URSI Commission B, and was an Associate Editor in *IEEE Transactions on Geoscience and Remote Sensing*. He serves as an Editorial Staff in *IEEE Antennas and Propagation Magazine*.



Wei Xiang Jiang was born in Jiangsu Province, China, in 1981. He received the B.S. degree in mathematics from Qingdao University in 2004, and the M.S. degree in applied mathematics in 2007 and Ph.D. degree in electrical engineering from Southeast University in 2010. His current research interests involve electromagnetic theory and metamaterials.



Qiang Cheng was born in Anhui Province, China, in 1979. He received the B.S. and M.S. degrees in electrical engineering from Nanjing University of Aeronautics and Astronautics in 2001 and 2004 respectively, and the Ph.D. degree from Southeast University in 2008. His current research interests involve electromagnetic theory, computational electromagnetics and metamaterials.



Hui Feng Ma was born in Jiangsu Province, China, on December 10, 1981. He received the B.S. degree in electrical engineering from the Nanjing University of Science and Technology, Nanjing, China, in 2004, and the Ph.D. degree in electromagnetic and microwave technology from Southeast University, Nanjing, China, in 2010. His research interests include design and analysis of microwave circuits and metamaterials.



Xiao-Yang Zhou was born in Jiangsu, China, in August 1979. He received the B.E. degree from the Air Force Institute of Radar, Wuhan, China, in 2001. He is currently working toward the Ph.D. degree at Southeast University, Nanjing, China. His research interests include numerical technique in electromagnetics and signal processing.



Xin Mi Yang was born in Jiangsu Province, P.R. China, in 1982. He received the B.S. and Ph.D. degrees from Southeast University, Nanjing, China, in 2005 and 2010, respectively, both in the School of Information Science and Engineering. Since November 2010, he has been with the School of Electronics and Information Engineering, Soochow University, Suzhou, P.R. China. His current research interests include metamaterials and their applications on antennas and microwave devices.